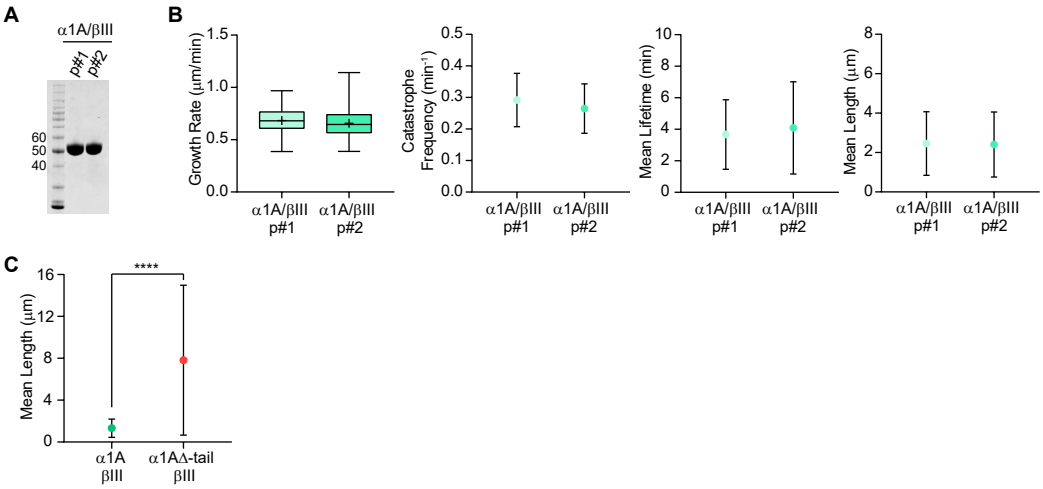


**Figure S1. Dynamic parameters are consistent between different preparations of recombinant human α1A/βIII tubulin (related to Figures 1 and 3).** (A) SDS-polyacrylamide gel (5 μgs) of recombinant human α1A/βIII from two different growths and purifications. (B) Plus-end dynamic parameters of α1A/βIII microtubules at 6 μM from the two different preparations shown in (A). From left to right: Growth rates in box-whisker plot (whiskers represent minimum to maximum); n= 256 and 95 growth phases for preparation #1 and preparation #2, respectively. Catastrophe frequencies; n= 29 and 12 microtubules for preparation #1 and preparation #2, respectively. Microtubule mean lifetime and mean length; n= 256 and 95 growth phases for preparation #1 and preparation #2, respectively. Error bars represent S.D. (C) Microtubule plus-end mean length at 4 μM tubulin concentration; n= 181 and 424 for α1A/βIII and α1AΔ-tail/βIII, respectively. Error bars represent S.D.; **** denotes $p < 0.0001$ as determined by a Mann-Whitney test.

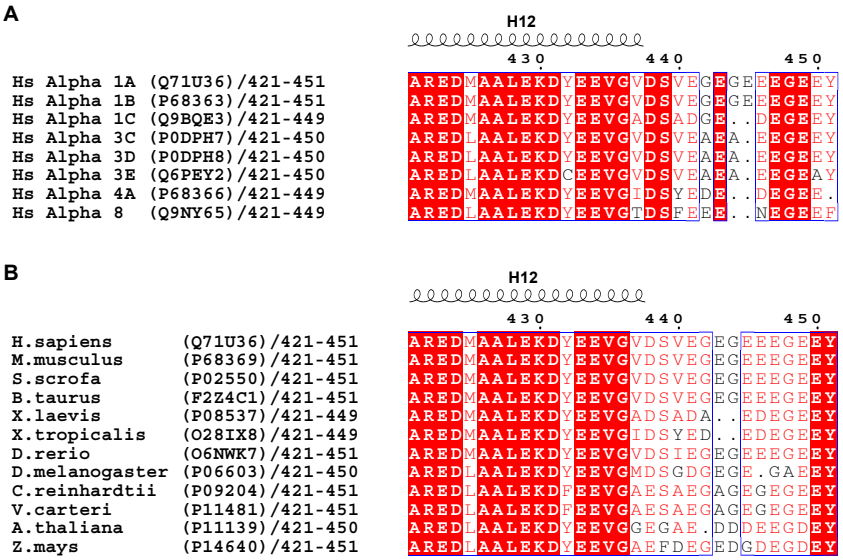


**Figure S2. Sequence alignment of α-tubulin tails (related to Figures 1 and 3).**
(A) Sequence alignment of the C-termini of eight human α-tubulin isotypes. Uniprot ID for each sequence indicated in brackets. The length of the H12 helix is based on the cryo-EM structure of human recombinant α1A/βIII microtubules (PDB ID: 5JCO; (Vemu, et al., 2016)). (B) Sequence alignment of tubulin α1A isotypes from various species.

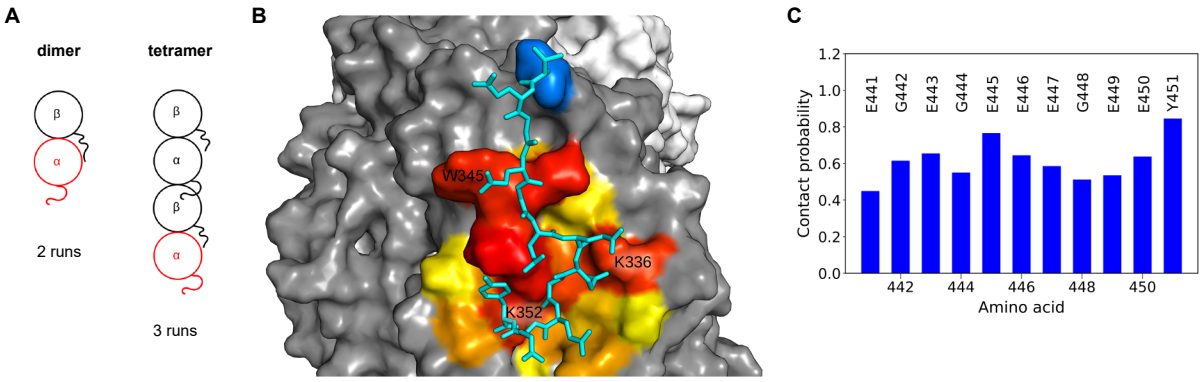


**Figure S3 (related to Figures 2 and 3).**
(A) Schematics of MD models used to examine the interactions between the tail of α-tubulin and its body. Red outline marks the α-tubulin subunit used in the analyses. (B) A snapshot of a simulation with a GTP-tubulin dimer, showing the α-tubulin tail interacting with positively charged residues at the α-tubulin longitudinal polymerization interface colored on a gradient from yellow to red according to the probability of its contact with the α-tubulin tail. Residue S439 where the tail originates is shown in blue. (C) Distribution of conditional contact probabilities for residues in the α-tubulin tail with the longitudinal polymerization interface, provided that at least one residue of the α-tubulin tail contacts the interface. Calculated from 5 independent one-micro-second-long simulations for GTP-tubulin.

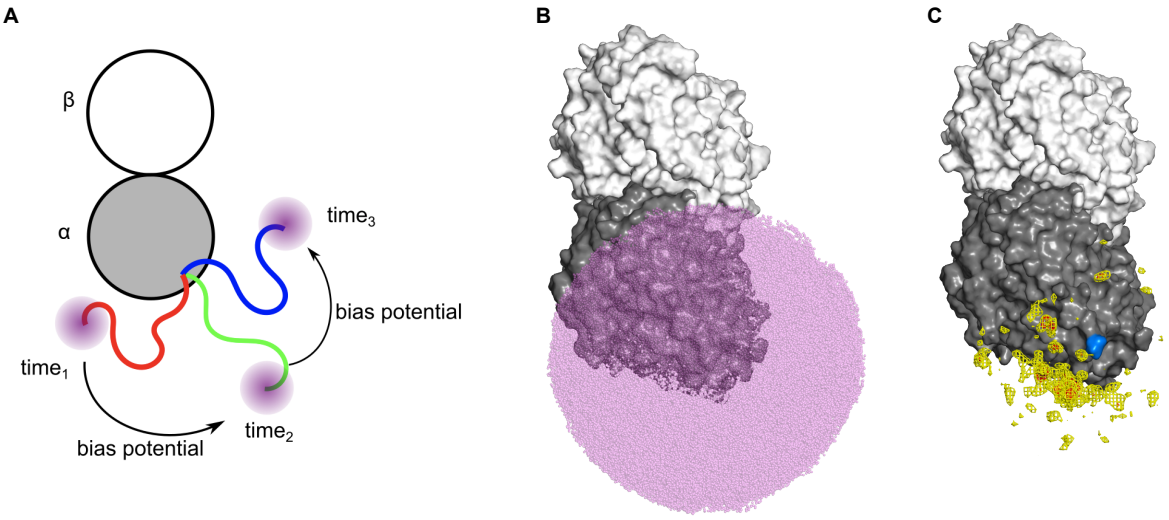


**Figure S4. Metadynamics simulation for enhanced sampling of the α-tubulin C-terminal tail (related to Figure 2).**
(A) Schematic of the metadynamics simulation. A bias potential (purple) is applied to the tip of the α-tubulin tail. Three configurations of the tail at three times are schematized. Bias potential accelerates displacement of the tail to enhance sampling of the configuration space. (B) A cloud of bias potentials (purple dots) added throughout the 2 μs-long metadynamics simulation. (C) Visualization of the positions where the highest densities of bias potentials were added to steer the C-terminal tip of the α-tubulin tail. The spatial distribution of these spots illustrates that the tail is predominantly located at the longitudinal polymerization interface. Residue S439 where the tail originates is shown in blue.

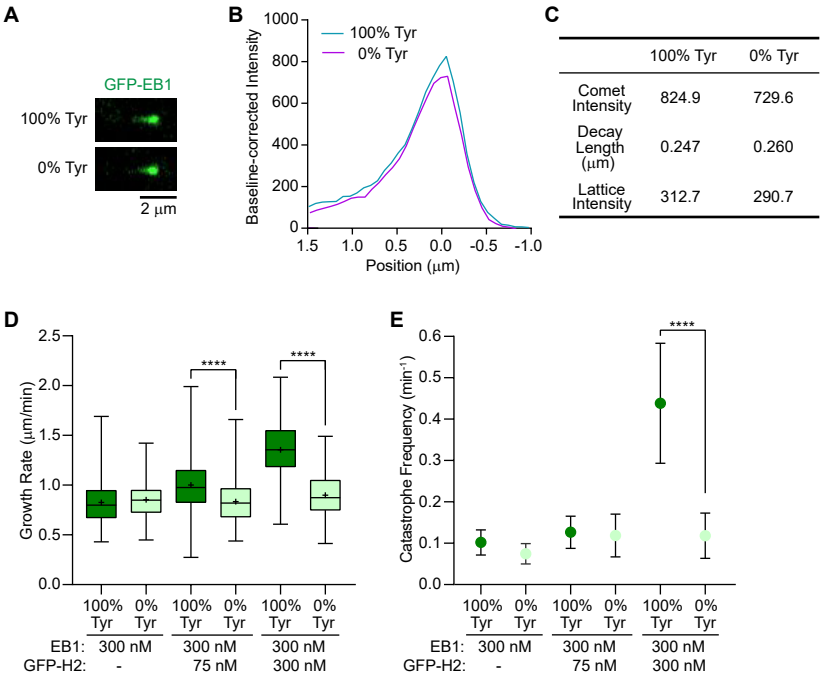


**Figure S5 (related to Figure 4)**

(A) TIRF microscopy images of GFP-EB1 (100 nM, green) on recombinant tyrosinated (100%) and detyrosinated (0%) microtubules. (B) Averaged fluorescence intensity profiles of GFP-EB1 (100 nM) on 15 μM tyrosinated (100%; n=124) or detyrosinated (0%; n=96) microtubules. (C) Comet profiles parameters. Comet profiles were fitted using Gaussian (-1.5 to 0 μm) and single exponential functions (0 to 1.5 μm; STAR Methods). (D, E) Plus-end dynamic parameters of 6 μM tyrosinated (100% Tyr) or detyrosinated (0% Tyr) microtubules in the presence of 300 nM EB1 and 0/75/300 nM GFP-H2. (D) Growth rates; n= 223, 82, 426, 309, 934, and 106 growth phases for 100%Tyr/EB1, 0%Tyr/EB1, 100%Tyr/EB1/H2 (75 nM), 0%Tyr/EB1/H2 (75 nM), 100%Tyr/EB1/H2 (300 nM), and 0%Tyr/EB1/H2 (300 nM), respectively. Whiskers represent minimum and maximum. (E) Catastrophe frequencies; n= 39, 17, 63, 50, 63, and 21 microtubules for 100%Tyr/EB1, 0%Tyr/EB1, 100%Tyr/EB1/H2 (75 nM), 0%Tyr/EB1/H2 (75 nM), 100%Tyr/EB1/H2 (300 nM), and 0%Tyr/EB1/H2 (300 nM), respectively. Error bars represent S.D.

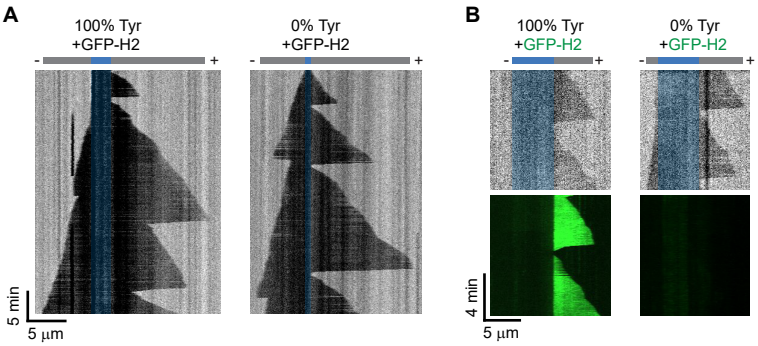


**Figure S6. CLIP-170 preferentially increases the rescue rates of tyrosinated microtubules (related to Figure 4).**
(A) Representative IRM kymographs of 6 μM 100% (left) or 0% (right) tyrosinated microtubules with 300 nM GFP-H2. (B) Representative IRM (top) and TIRF microscopy (bottom) kymographs of 6 μM tyrosinated (100% Tyr; left) or detyrosinated (0% Tyr; right) microtubules with 300 nM GFP-H2 (green).